Chapter 2
Literature Review

Photostrictive effect is a combination of photovoltaic effect (electric field generated under uniform illumination) and converse-piezoelectric effect (strain induced by an applied electric field). Photostrictive materials convert light directly to the physical movement.[4] When homogeneous non-centrosymmetric materials, such as ferroelectric single crystals and polarized ferroelectric ceramics, are uniformly illuminated, a high voltage that considerably exceeds the band gap energies is generated without an external field which resulted into a mechanical strain due to the converse-piezoelectric effect.

One compositional system that embraces both photovoltaic and converse-piezoelectric effects is lead lanthanum zirconate titanate (PLZT) which is a typical photostrictive material owing to its relatively high photostrictive efficiency and ease of preparation. The characteristics of photostrictive PLZT ceramics are presented in this chapter.

2.1 Perovskite structure ABO_3 : PLZT

The solid solution system, that forms the basis of PLZT materials, is a series of compositions resulted from the complete miscibility of lead zirconate and lead titanate in each other and modified by the solubility of substantial amounts of lanthanum oxide in the crystal lattice. A general formula for all compositions of the PLZT system is

$$Pb_{1-x}La_x(Zr_yTi_{1-y})_{1-x/4}O_3 \qquad (2.1)$$

where lanthanum ions replace lead ions in the A-site of perovskite ABO_3 ionic structure as shown in Fig. 2.1. Since La^{3+} substitutes for Pb^{2+}, electrical neutrality is maintained by the creation of lattice B-site vacancies.[4-9]

PLZT ceramics are currently focused because of their excellent piezoelectric properties and high piezoelectric constant (d_{33}) value. The compositions around the morphotropic phase boundary (MPB), between the tetragonal and rhombohedral phases, show the maximum d_{33} value.

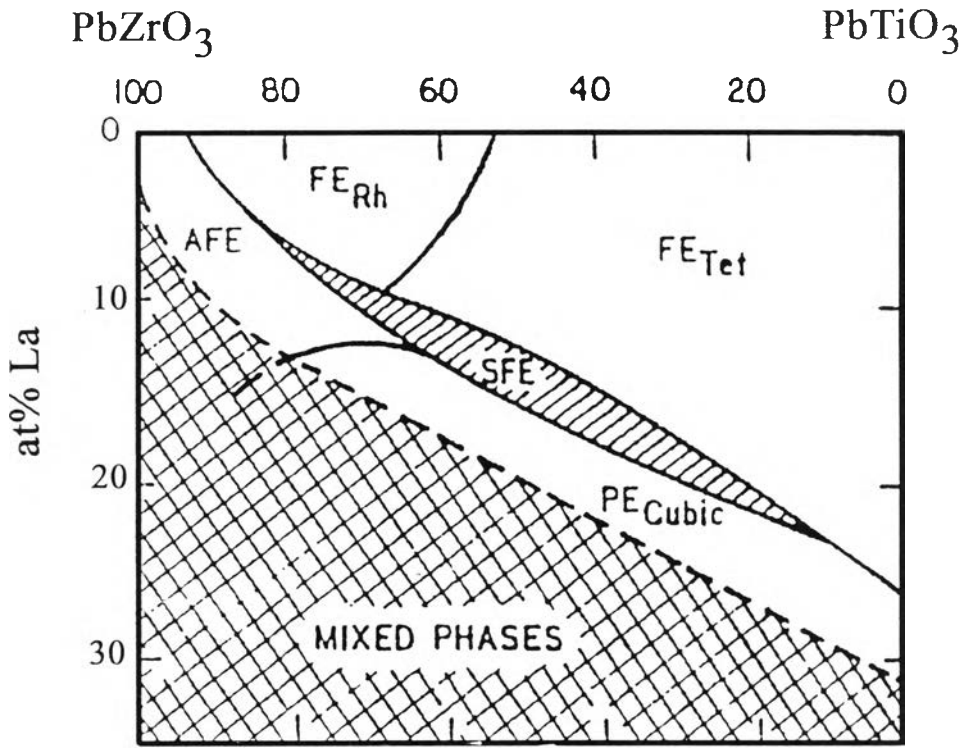

Fig. 2.1 Phase equilibrium diagram for $PbZrO_3$-$PbTiO_3$-La_2O_3 solid solution (PLZT)

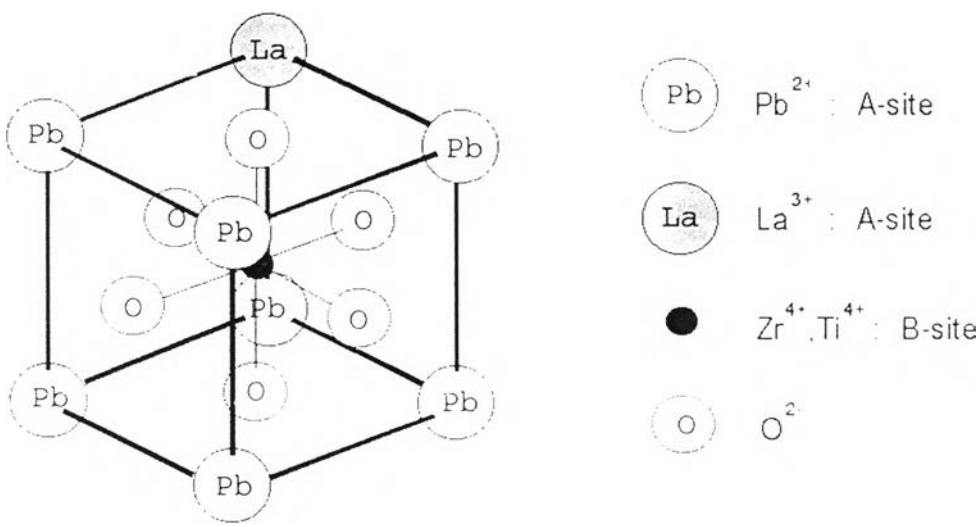

Fig. 2.2 PLZT Perovskite structure

Commonly, the excessive PbO about 2 at% contributes to achieve full density by forming a liquid phase at the grain boundaries and by inhibiting grain growth during the initial states of densification. Both of these effects are beneficial to the attainment of a theoretical dense material by eliminating residual porosity before it becomes entrapped within the grain.

2.1.1 Modeling of A- and B-site substitution

To improve properties of PLZT ceramics, such as sinterability, transparency, dielectric constant, quality factor, piezoelectric coefficient, and etc, a small amount of dopants is added. Previous work showed that dopant addition influenced the microstructure, physical properties and electrical properties of PLZT ceramics.[10] The lattice site substitution of doping ions can be predicted by the following method.[11]

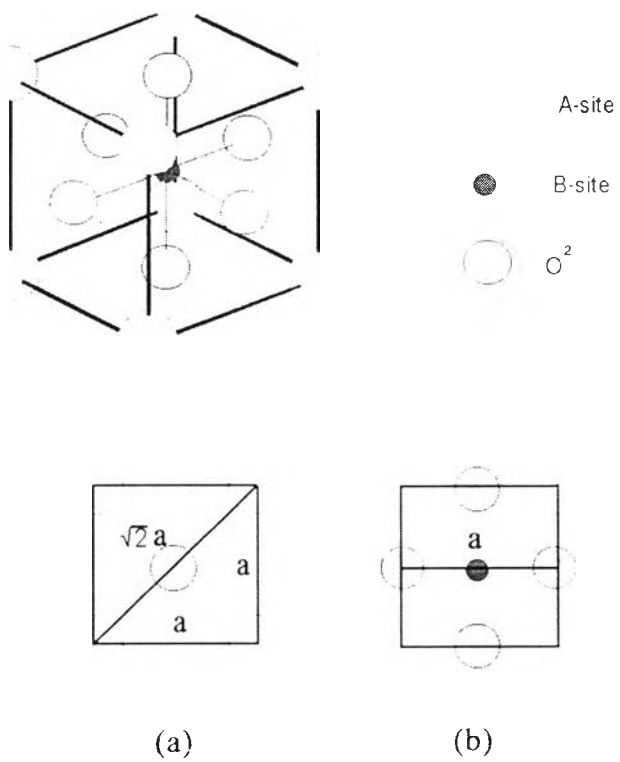

Fig. 2.3 Cubic perovskite structure and geometrical considerations for lattice parameter "a".[11]

The ABO_3 perovskite structure of PLZT is shown in Fig. 2.2. It can be described geometrically as shown in Fig. 2.3. The A- and B-site cations are 12 and 6-coordinated, respectively. The A-site cation is normally larger than that of the B-site. The oxygen anion has a coordination number of 6. Assuming that all the ions are hard spheres, the lattice parameter "**a**" of the cubic perovskite is given by

$$a = 2 (r_{A(12\text{-}CN)} + r_{O(6\text{-}CN)}) / \sqrt{2} \qquad (2.2)$$

or

$$a = 2 (r_{B(6\text{-}CN)} + r_{O(6\text{-}CN)}) \qquad (2.3)$$

as shown in Fig. 2.3 (a) and (b). Here, $r_{A(12\text{-}CN)}$, $r_{B(6\text{-}CN)}$, and $r_{O(6\text{-}CN)}$ are the ionic radii of the 12-coordinated A-site cation, 6-coordinated B-site cation, and 6-coordinated oxygen anion, respectively. The stability of the perovskite structure can also be described geometrically as the ratio of Eq. 2.2 to 2.3 which is defined as the Tolerance Factor (t)

$$t = \frac{(r_{A(12\text{-}CN)} + r_{O(6\text{-}CN)})}{\sqrt{2} (r_{B(6\text{-}CN)} + r_{O(6\text{-}CN)})} \qquad (2.4)$$

It is advantageous that the A- and B-site cations are in contact with oxygen anions for an ABO_3 compound to form a stable perovskite structure. That is, the perovskite structure is more stable if $t \approx 1.0$.

When a foreign cation is introduced into the perovskite sub-lattice, the substitution site of the cation is determined mainly by two factors: charge and size. In this study, the assumption has been made which based on all the selected ions able to be replaced either in the divalent A-site or in the tetravalent B-site. However, the values of ionic radii illustrated in Table. 2.1 show that large and small ions are likely to occupy A and B-sites, respectively. As a result, the unit-cell formula in the PLZT series is expected to vary with the additives of substitutions. There are three factors, which are considered in calculating the unit-cell formula for this research.

(1) Mass and charge balances must be maintained.
(2) The La : Dopant : Zr : Ti atomic ratio is 3 : 0.5 : 52 : 48
(3) It is assumed that the vacancy occurred on only B-site

when M^{v+} ions (M is the added metal cation, v is valency) enter the A-site (A-site substitution for Pb^{2+}), the unit-cell formula can be readily calculated as

$$(Pb_{0.965}La_{0.03}M_{0.005})[(Zr_{0.52}Ti_{0.48})_{1-0.03/4+0.005(2-v)/4}V_{0.03/4+0.005(2-v)/4}]O_3 \qquad (2.5)$$

where V is vacancy
whereas the B-site substitution, the unit-cell formula can be calculated as

$$(Pb_{0.97}La_{0.03})[(Zr_{0.52}Ti_{0.48})_{1-0.03/4+0.005(4-v)/4-0.005}M_{0.005}V_{0.03/4+0.005(4-v)/4-0.005}]O_3 \qquad (2.6)$$

For example, the formula for K^+ substitutes on A-site is

$(Pb_{0.965}La_{0.03}K_{0.005})(Zr_{0.51675}Ti_{0.477}V_{0.00625})O_3$.

for B-site substitution, the formula is

$(Pb_{0.97}La_{0.03})(Zr_{0.51545}Ti_{0.4758}K_{0.005}V_{0.00375})O_3$.

These formulas will be used in theoretical calculation of physical and structural properties, such as formula weight, tolerance factor, theoretical density, and A or B lattice site substitution.

2.1.2 Calculations of tolerance factor

The effective ionic radii suggested by Moulson (1990)[12] and Shannon (1974)[13] as shown in Table. 2.1. are used to calculate the tolerance factor. However, the $r_{M(6\text{-}CN)}$ and $r_{M(12\text{-}CN)}$ values for several metal ions have not been reported. The known $r_{M(6\text{-}CN)}$ and $r_{M(12\text{-}CN)}$ values have been estimated simply by multiplying the known $r_{M(X\text{-}CN)}$

value by the ratio (i.e., 1.127) of $r_{La(12\text{-}CN)} : r_{La(8\text{-}CN)}$ for La^{3+}. Since the $r_{Y(8\text{-}CN)}$ of Y^{3+} is 102 pm [12], the estimation of $r_{Y(12\text{-}CN)}$ will be 115 pm. Moreover, the radii of B-site vacancy have been assumed to be equal to the average radii of B-site cations.

The tolerance factor for both A- and B-site substitutions is based on the assumption that substitution in A-site creates only B-site vacancy (Table 2.2) and substitution in B-site also creates B-site vacancy (Table 2.3). The unit cell formulas of PLZT doped with various metal ions listed in Table 2.4 have been calculated according to Eq. 2.4 taking into account that all the tolerance factors are < 1.0.

2.1.2 Determination of substitution site of doping ions

The tolerance factor of the A-site substitution formula for ions larger than 115 pm (12-CN) is closer to 1.0 than those of the B-site substitution formula (Table. 2.4). The A-site substitution is therefore expected to be more favorable for large ions while the B-site substitution is favorable for ions smaller than 115 pm (12-CN).

Park, et al.[11] calculated the tolerance factors to determine the dopant distribution between A-and B-sites in PLZT (5/63/37) ceramics modified by lanthanide ions (Ln^{3+}). They concluded that the distribution seemed to be a regular function of the ionic radius of the lanthanide. The A-site substitution was predominant for large Ln^{3+} ions while the B-site substitution was predominant for small Ln^{3+} ions. A- and B-site substitutions could occur simultaneously for Ln^{3+} ions with intermediate size. Therefore, the size of Ln^{3+} ion had significant effect on their substitution site and structural properties.

In this study, several metal cations were selected to investigate the effect of additives on the photostrictive properties of PLZT ceramics.

Table 2.1 Selected ion, atomic number, electron configuration, and ionic radii for doped PI ZT series.

Ion	Atomic No.	Configuration	valency	Ionic radii (pm)	
				A-site CN. = 12	B-site CN. = 6
B^{3+}	5	$[He]2s^2 2p^1$	3	20 [e]	16 [c]
Ba^{2+}	56	$[Xe]6d^2$	2	159 [a]	136 [a]
Bi^{3+}	83	$[Xe]4f^{14}5d^{10}6s^2 6p^3$	3	127 [f]	102 [a]
Co^{2+}	27	$[Ar]3d^7 4s^2$	2	79 [d]	58 [a]
Cr^{3+}	24	$[Ar]3d^5 4s^1$	3	76 [f]	62 [a]
Cu^{2+}	29	$[Ar]3d^{10}4s^1$	2	98 [d]	72 [a]
Fe^{3+}	26	$[Ar]3d^6 4s^2$	3	69 [f]	56 [a]
Gd^{3+}	64	$[Xe]4f^7 5d^1 6s^2$	3	118 [f]	96 [f]
K^+	19	$[Ar]4s^1$	1	160 [a]	136 [a]
Li^+	3	$1s^2 2s^1$	1	88 [c]	75 [a]
Mn^{3+}	25	$[Ar]3d^5 4s^2$	3	71 [f]	58 [a]
Nb^{5+}	41	$[Kr]4d^4 5s^1$	5	80 [f]	65 [a]
Ni^{2+}	28	$[Ar]3d^8 4s^2$	2	94 [d]	69 [a]
Se^{4+}	34	$[Ar]3d^{10}4s^2 4p^4$	4	62 [f]	50 [b]
Sn^{4+}	50	$[Kr]4d^{10}5s^2 5p^2$	4	85 [f]	69 [a]
Sr^{2+}	38	$[Kr]5s^2$	2	144 [a]	117 [a]
V^{5+}	23	$[Ar]3d^3 4s^2$	5	68 [f]	55 [a]
W^{6+}	74	$[Xe]4f^{14}5d^4 6s^2$	6	70 [f]	58 [a]
Y^{3+}	39	$[Kr]4d^1 5s^2$	3	115 [f]	93 [a]
Zn^{2+}	30	$[Ar]3d^{10}4s^2$	2	103 [d]	76 [a]
Pb^{2+}	82	$[Xe]4f^{14}5d^{10}6s^2 6p^2$	2	150 [a]	
La^{3+}	57	$[Xe]5d^1 6s^2$	3	133 [a]	
Zr^{4+}	40	$[Kr]4d^2 5s^2$	4		73 [a]
Ti^{4+}	22	$[Ar]3d^2 4s^2$	4		60 [a]
O^{2-}	8	$1s^2 2s^2 2p^4$	-2		140 [a]

[a] Moulson, A. (1990)[12]

[b] Shannon, R.D. (1974)[15]

[c] These 12-coordinated ionic radii were calculated by multiplying the known 6-coordinated radii by the $r_{K(12\text{-}CN)} : r_{K(6\text{-}CN)}$ ratio, which were known.

[d] These 12-coordinated ionic radii were calculated by multiplying the known 6-coordinated radii by the $r_{Ca(12\text{-}CN)} : r_{Ca(6\text{-}CN)}$ ratio, which were known.

[e] These 12-coordinated ionic radii were calculated by multiplying the known 6-coordinated radii by the $r_{Al(12\text{-}CN)} : r_{Al(6\text{-}CN)}$ ratio, which were known.

[f] These 12-coordinated ionic radii were calculated by multiplying the known 6-coordinated radii by the $r_{La(12\text{-}CN)} : r_{La(6\text{-}CN)}$ ratio, which were known.[11,12]

Table 2.2 Formula of doped PLZT ceramics with an assumption of substitution in A-site creating B-site vacancy.

Ion	Formula
B^{3+}	$(Pb_{0.965}La_{0.03}B_{0.005})(Zr_{0.51545}Ti_{0.4758}V_{0.00875})O_3$
Ba^{2+}	$(Pb_{0.965}La_{0.03}Ba_{0.005})(Zr_{0.5161}Ti_{0.4764}V_{0.0075})O_3$
Bi^{3+}	$(Pb_{0.965}La_{0.03}Bi_{0.005})(Zr_{0.51545}Ti_{0.4758}V_{0.00875})O_3$
Co^{2+}	$(Pb_{0.965}La_{0.03}Co_{0.005})(Zr_{0.5161}Ti_{0.4764}V_{0.0075})O_3$
Cr^{3+}	$(Pb_{0.965}La_{0.03}Cr_{0.005})(Zr_{0.51545}Ti_{0.4758}V_{0.00875})O_3$
Cu^{2+}	$(Pb_{0.965}La_{0.03}Cu_{0.005})(Zr_{0.5161}Ti_{0.4764}V_{0.0075})O_3$
Fe^{3+}	$(Pb_{0.965}La_{0.03}Fe_{0.005})(Zr_{0.51545}Ti_{0.4758}V_{0.00875})O_3$
Gd^{3+}	$(Pb_{0.965}La_{0.03}Gd_{0.005})(Zr_{0.51545}Ti_{0.4758}V_{0.00875})O_3$
K^{+}	$(Pb_{0.965}La_{0.03}K_{0.005})(Zr_{0.51675}Ti_{0.477}V_{0.00625})O_3$
Li^{+}	$(Pb_{0.965}La_{0.03}Li_{0.005})(Zr_{0.51675}Ti_{0.477}V_{0.00625})O_3$
Mn^{3+}	$(Pb_{0.965}La_{0.03}Mn_{0.005})(Zr_{0.51545}Ti_{0.4758}V_{0.00875})O_3$
Nb^{5+}	$(Pb_{0.965}La_{0.03}Nb_{0.005})(Zr_{0.51415}Ti_{0.4746}V_{0.01125})O_3$
Ni^{2+}	$(Pb_{0.965}La_{0.03}Ni_{0.005})(Zr_{0.5161}Ti_{0.4764}V_{0.0075})O_3$
Se^{4+}	$(Pb_{0.965}La_{0.03}Se_{0.005})(Zr_{0.5148}Ti_{0.4752}V_{0.01})O_3$
Sn^{4+}	$(Pb_{0.965}La_{0.03}Sn_{0.005})(Zr_{0.5148}Ti_{0.4752}V_{0.01})O_3$
Sr^{2+}	$(Pb_{0.965}La_{0.03}Sr_{0.005})(Zr_{0.5161}Ti_{0.4764}V_{0.0075})O_3$
V^{5+}	$(Pb_{0.965}La_{0.03}V_{0.005})(Zr_{0.51415}Ti_{0.4746}V_{0.01125})O_3$
W^{6+}	$(Pb_{0.965}La_{0.03}W_{0.005})(Zr_{0.5135}Ti_{0.474}V_{0.0125})O_3$
Y^{3+}	$(Pb_{0.965}La_{0.03}Y_{0.005})(Zr_{0.51545}Ti_{0.4758}V_{0.00875})O_3$
Zn^{2+}	$(Pb_{0.965}La_{0.03}Zn_{0.005})(Zr_{0.5161}Ti_{0.4764}V_{0.0075})O_3$

Table 2.3 Formula of doped PLZT ceramics with an assumption of substitution in B-site creating B-site vacancy.

Ion	Formula
B^{3+}	$(Pb_{0.97}La_{0.03})(Zr_{0.51415}Ti_{0.4746}B_{0.005}V_{0.00625})O_3$
Ba^{2+}	$(Pb_{0.97}La_{0.03})(Zr_{0.5148}Ti_{0.4752}Ba_{0.005}V_{0.005})O_3$
Bi^{3+}	$(Pb_{0.97}La_{0.03})(Zr_{0.51415}Ti_{0.4746}Bi_{0.005}V_{0.00625})O_3$
Co^{2+}	$(Pb_{0.97}La_{0.03})(Zr_{0.5148}Ti_{0.4752}Co_{0.005}V_{0.005})O_3$
Cr^{3+}	$(Pb_{0.97}La_{0.03})(Zr_{0.51415}Ti_{0.4746}Cr_{0.005}V_{0.00625})O_3$
Cu^{2+}	$(Pb_{0.97}La_{0.03})(Zr_{0.5148}Ti_{0.4752}Cu_{0.005}V_{0.005})O_3$
Fe^{3+}	$(Pb_{0.97}La_{0.03})(Zr_{0.51415}Ti_{0.4746}Fe_{0.005}V_{0.00625})O_3$
Gd^{3+}	$(Pb_{0.97}La_{0.03})(Zr_{0.51415}Ti_{0.4746}Gd_{0.005}V_{0.00625})O_3$
K^{+}	$(Pb_{0.97}La_{0.03})(Zr_{0.51545}Ti_{0.4758}K_{0.005}V_{0.00375})O_3$
Li^{+}	$(Pb_{0.97}La_{0.03})(Zr_{0.51545}Ti_{0.4758}Li_{0.005}V_{0.00375})O_3$
Mn^{3+}	$(Pb_{0.97}La_{0.03})(Zr_{0.51415}Ti_{0.4746}Mn_{0.005}V_{0.00625})O_3$
Nb^{5+}	$(Pb_{0.97}La_{0.03})(Zr_{0.51285}Ti_{0.4734}Nb_{0.005}V_{0.00875})O_3$
Ni^{2+}	$(Pb_{0.97}La_{0.03})(Zr_{0.5148}Ti_{0.4752}Ni_{0.005}V_{0.005})O_3$
Se^{4+}	$(Pb_{0.97}La_{0.03})(Zr_{0.5135}Ti_{0.474}Se_{0.005}V_{0.0075})O_3$
Sn^{4+}	$(Pb_{0.97}La_{0.03})(Zr_{0.5135}Ti_{0.474}Sn_{0.005}V_{0.0075})O_3$
Sr^{2+}	$(Pb_{0.97}La_{0.03})(Zr_{0.5148}Ti_{0.4752}Sr_{0.005}V_{0.005})O_3$
V^{5+}	$(Pb_{0.97}La_{0.03})(Zr_{0.51285}Ti_{0.4734}V_{0.005}V_{0.00875})O_3$
W^{6+}	$(Pb_{0.97}La_{0.03})(Zr_{0.5122}Ti_{0.4728}W_{0.005}V_{0.01})O_3$
Y^{3+}	$(Pb_{0.97}La_{0.03})(Zr_{0.51415}Ti_{0.4746}Y_{0.005}V_{0.00625})O_3$
Zn^{2+}	$(Pb_{0.97}La_{0.03})(Zr_{0.5148}Ti_{0.4752}Zn_{0.005}V_{0.005})O_3$

Table 2.4 Calculated average ionic radii of A- and B-site substitution. The tolerance factor is calculated and used to determine the substitution site and the effect of additives.[2,14-21]

Ion	A-site substituted			B-site substituted			Site	effect
	$r_{A(12\text{-}CN)}$	$r_{B(6\text{-}CN)}$	tolerance	$r_{A(12\text{-}CN)}$	$r_{B(6\text{-}CN)}$	tolerance		
B^{3+}	148.84	66.76	0.9878	149.49	66.50	0.9913	B	acceptor
Ba^{2+}	149.54	66.76	0.9902	149.49	67.11	0.9884	A	isovalence
Bi^{3+}	149.38	66.76	0.9896	149.49	66.94	0.9892	A	donor
Co^{2+}	149.14	66.76	0.9888	149.49	66.72	0.9902	B	acceptor
Cr^{3+}	149.12	66.76	0.9888	149.49	66.74	0.9902	B	acceptor
Cu^{2+}	149.23	66.76	0.9891	149.49	66.79	0.9899	B	acceptor
Fe^{3+}	149.09	66.76	0.9887	149.49	66.71	0.9903	B	acceptor
Gd^{3+}	149.33	66.76	0.9895	149.49	66.91	0.9893	A	donor
K^{+}	149.54	66.76	0.9902	149.49	67.11	0.9884	A	acceptor
Li^{+}	149.18	66.76	0.9890	149.49	66.80	0.9898	B	acceptor
Mn^{3+}	149.10	66.76	0.9887	149.49	66.72	0.9902	B	acceptor
Nb^{5+}	149.14	66.76	0.9888	149.49	66.75	0.9901	B	donor
Ni^{2+}	149.21	66.76	0.9891	149.49	66.77	0.9900	B	acceptor
Se^{4+}	149.05	66.76	0.9885	149.49	66.68	0.9904	B	isovalence
Sn^{4+}	149.17	66.76	0.9889	149.49	66.77	0.9900	B	isovalence
Sr^{2+}	149.46	66.76	0.9899	149.49	67.01	0.9888	A	isovalence
V^{5+}	149.08	66.76	0.9886	149.49	66.70	0.9903	B	donor
W^{6+}	149.09	66.76	0.9887	149.49	66.72	0.9903	B	donor
Y^{3+}	149.32	66.76	0.9895	149.49	66.89	0.9894	A	donor
Zn^{2+}	149.26	66.76	0.9892	149.49	66.81	0.9898	B	acceptor

Remark : Tolerance factor of PLZT (3/52/48) = 0.9900 (La^{3+} substitutes in A-site creating B-site vacancy only)

From the calculation of tolerance factor in Table 2.4, the selected ions can be divided into following five groups.

1. Donor B-site : Nb^{5+}, W^{6+}
2. Donor A-site : Bi^{3+}, Gd^{3+}, Y^{3+}
3. Isovalence : Ba^{2+}, Sr^{+2}, Se^{4+}, Sn^{4+}
4. Acceptor : B^{3+}, Li^{+}, K^{-}
5. 3d transition : Cr^{3+}, Cu^{2+}, Fe^{3+}, Mn^{3+}, Ni^{2+}, V^{5+}, Co^{2+}, Zn^{2+}

2.2 Photovoltaic effect

2.2.1 Background

In solar cell technologies, photoelectric or photovoltaic cells convert sunlight directly into electricity. Photovoltaic cells are the solar cells that are often used to power calculators and watches. They are made of semiconducting materials similar to those used in computer chips. When sunlight is absorbed by these materials, light striking such crystals as silicon or germanium, in which electrons are usually not free to move from atom to atom within the crystal, provides the energy needed to free some electrons from their bound condition. Free electrons cross the junction between two dissimilar crystals (p-n junction) more easily in one direction than in the other, giving one side of the junction a negative charge and, therefore, a negative voltage with respect to the other side, allowing the electrons to flow through the material to produce electricity. The photovoltaic battery can continue to provide voltage and current as long as light continues to fall on the two materials. Fig. 2.4 illustrates the schematic diagram of a photovoltaic model in p-n junctions.

Photovoltaic effect in ferroelectrics is different from the corresponding phenomenon in p-n junction of semiconductors. When ferroelectric material is irradiated with photons having energy corresponding to the band gap of the material, steady state short-circuit current and open-circuit voltage are generated. The photovoltaic effect is observed only along the direction of the spontaneous polarization (P_s).

The generated voltage proportional to the sample length along the P_s direction is on the order of kV/cm to MV/cm, referred to as the Anomalous Photovoltage Effect (APE) or the Bulk Photovoltaic Effect (BPE).[22-25] An interesting anomalous photovoltaic effect in $BaTiO_3$[25], $LiNbO_3$[22] single crystals, and PLZT polycrystallines was first observed.

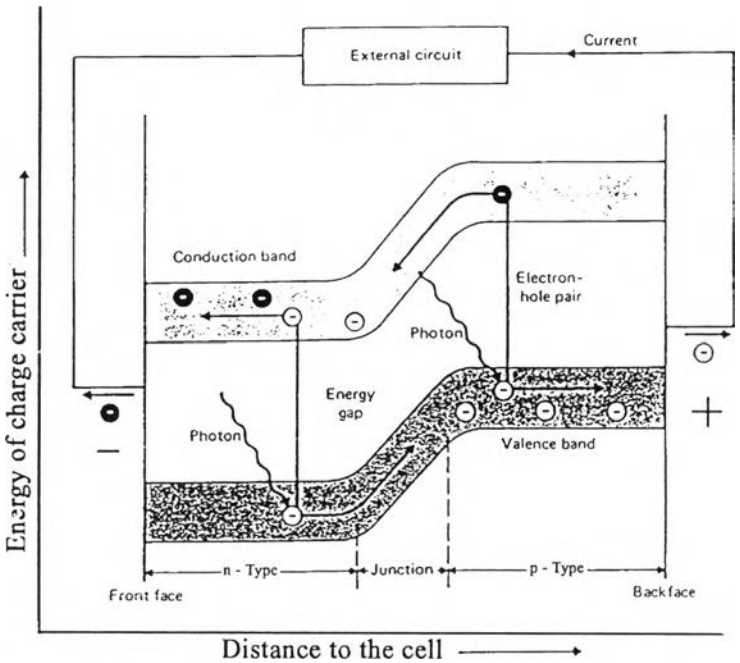

Fig. 2.4 Simple photovoltaic effect model for p-n junction solar energy

The production of such a high photovoltage is not only of interest theoretically, but also of considerable practical importance. Photo-driven actuators and optical control modulators, which enable wireless remote control and all-optical operation, are some of the photovoltaic devices.[1,26-28]

2.2.2 Effect of additive ions on photovoltaic properties of PLZT ceramics

The effect of additive ions[29,30] on the electronic properties (donor/acceptor mechanism) of PLZT[31] ceramics was clearly explained by three types of additives.[32]

Donor additives, such as Nb^{5+} replacing Zr^{4+} or La^{3+} replacing Pb^{2+}, counteract the natural p-type conductivity of PZT ceramics and thus raise the electrical resistivity. They are usually compensated by cation-site vacancies. These additives enhance domain reorientation. Ceramics doped with these additives are characterized by square hysteresis loops, low coercivity, high remnant polarization, high dielectric constant, maximum coupling factors, high dielectric loss, high compliance, and reducing aging. Typical applications are in the area of high sensitivity, such as hydrophones, photograph pickups, sounders and loudspeaker.

Acceptor additives, such as Cu^{2+} replacing Zr^{4+} or K^{+} replacing Pb^{2+}, are compensated by oxygen vacancies and usually have only limited solubility in the lattice. Domain reorientation is limited, and hence ceramics with acceptor additives are characterized by poorly developed hysteresis loops, lower dielectric constant[10], low dielectric loss, low compliance and high aging rates. Typical applications are in high-power devices such as sonar and ultrasonic transducer.

Isovalent additives, such as Ba^{2+} or Sr^{2+} replacing Pb^{2+} or Sn^{4+} replacing Zr^{4+}, in which the substituting ions are of the same valency and approximately the same size as the replaced ion. Solid solution consisting these additives are usually resulted in lower Curie points. Hysteresis loops may be poorly developed without an additional additive. Other properties include lower dielectric loss, low compliance, and higher aging rate. These ceramics are used in high-drive applications.

It has been proposed that the valence of dopants will significantly affect the photovoltaic response. It is believed that most of doping ions are incorporated. The photovoltaic response for various dopants with the same condition of 1 at% doped PLZT (3/52/48) was investigated by Tanimura (1988).[2] A dashed line in Fig. 2.5 represents the constant of photovoltaic power curve corresponding to the undoped PLZT ceramics. Donor doping on to the B-site (Nb^{5+}, Ta^{5+}, W^{6+}) enhances the photovoltaic response.

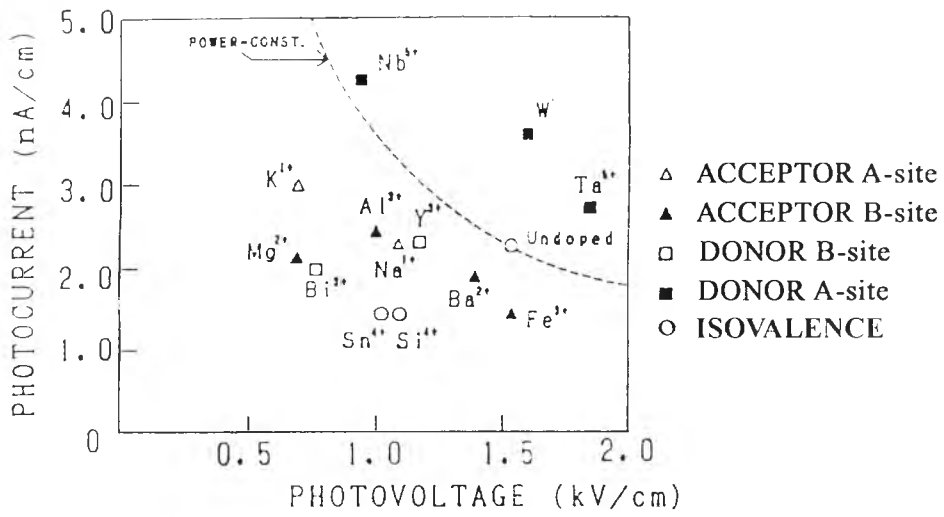

Fig. 2.5 Photovoltaic response as a function of doping ions

2.2.3 Effect of composition on photovoltaic properties of PLZT ceramics.

Photovoltaic properties of PLZT ceramics had been found to depend on their composition.[1,3,33-38] The optimum properties were found in the composition along the Morphotropic Phase Boundary (MPB). The studies of Uchino in 1985 focused on optimizing the compositional variation along the MPB, the maximum photovoltaic properties were obtained from the PLZT ceramics (3/52/48). Fig. 2.6 shows the contouring map of photovoltaic effect in PLZT system. A dark line in the figure is the MPB and a dashed line is the iso-power line (product of photocurrent and photovoltage).

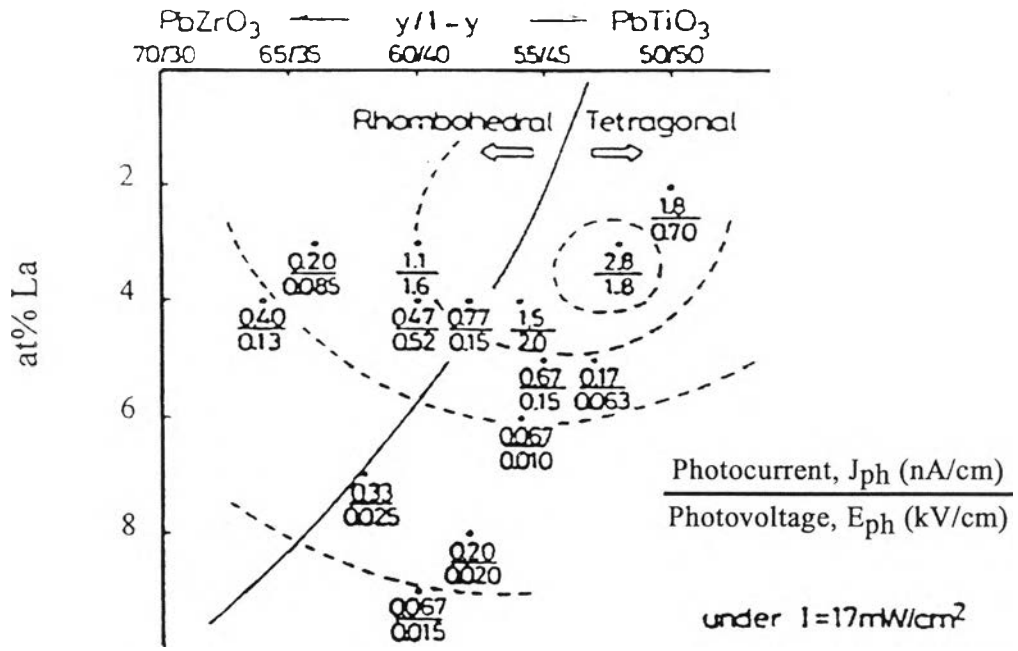

Fig. 2.6 Contour map of photovoltaic response in PLZT system

2.2.4 Effect of light wavelength on photovoltaic properties

Optical absorption in PLZT ceramics is wavelength dependent, becoming extremely high in the violet (short wavelength)[39] end of the spectrum near 370-380 nm. The relationship between optical transmission with wavelength in different PLZT ceramics composition is shown in Fig. 2.7 [40]

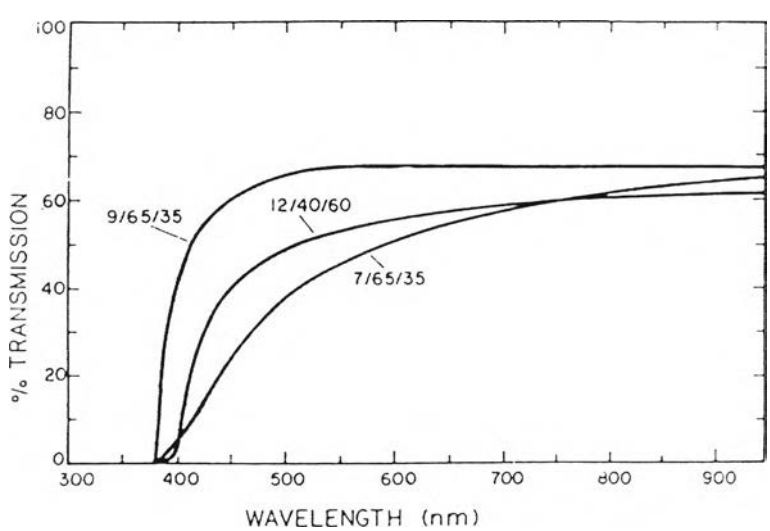

Fig. 2.7 Optical transmission spectra characteristic of PLZT ceramics

Uchino (1988)[2] proposed the band gap energy (E_g) model of PLZT ceramics as shown in Fig. 2.8. Donor doping addition into PLZT will form the donor level which is possible to change the band gap energy of PLZT ceramics.

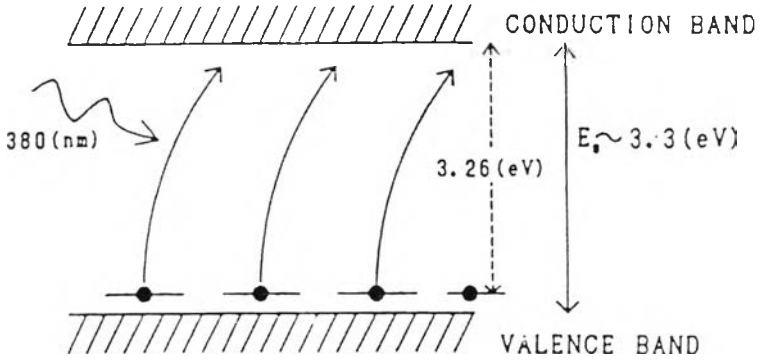

Fig. 2.8 Band gap energy (E_g) model for PLZT ceramics

The optical absorption edge or the band gap energy can be determined from the optical transmission spectra, which can be converted to the absorption coefficient by

$$\% \text{ transmission} = I / I_0 \times 100$$

and

$$I / I_0 = \exp(- \alpha d) \qquad (2.7)$$

where I and I_0 represent the transmitted and incident light intensities, d is thickness of specimens, and α is an absorption coefficient.

Analysis of the optical spectra is one of the most productive tools for understanding the band gap energy of materials. The optical absorption curve of materials consists of three parts.[41]

1. A high absorption region ($\alpha \geq 104$ cm^{-1}) where assuming parabolic band edges and energy independent matrix element for the interband transitions, the absorption coefficient α is then given by [41,42]

Direct band gap : $\alpha h\nu = A (h\nu - E_g)^{1/2}$ (2.8)

Indirect band gap : $\alpha h\nu = A (h\nu - E_g)^{2}$ (2.9)

In which $h\nu$, E_g, and A, B denote the photon energy, optical band gap energy, and constants, respectively.

2. An intermediate absorption range ($1\ cm^{-1} < \alpha < 10^4\ cm^{-1}$) in which the absorption depends exponentially on the photon energy :

$$\alpha h\nu = \alpha_0 \exp (h\nu / E_0) \quad (2.10)$$

with a slope parameter, E_0, which usually falls between 0.05 and 0.08 eV and is defined as the width of band tails of localized states into the gap.

3. A weak absorption tail at low absorption constants ($\alpha < 10^{-1}$ cm^{-1}) whose shape and magnitude depend on the purity, thermal history, and preparation conditions.

Although it appears valid for certain well-studied semiconductors, this approach may not be precise for wide-band gap oxide and perovskite ceramics such as TiO_2[43-45], $BaTiO_3$[25,46,47], $SrTiO_3$[13], PSN[48], PZT, and PLZT[22,23,48,49]

Calculation of band structure indicates that the perovskite structure materials can not be easily identified as either direct or indirect band gap semiconductors.[46] Large conduction zone anisotropy and nearly flat zone regions that lead to two-dimensional conduction band may render the parabolic conduction band approximation invalid. Optical band gap value obtained in this way may not be precise and may only be useful for the comparison between materials.

From the comparison between the optical transmission method[49] and wavelength dependent photocurrent method[4,23] (Fig. 2.10), it can be concluded that the indirect band gap would be the band structure of

PLZT ceramics. Due to this assumption, the band gap energy is formally defined as the intercept of the curve $(\alpha\ h\ \nu)^{1/2}$ vs $h\nu$ as shown in Fig. 2.9.

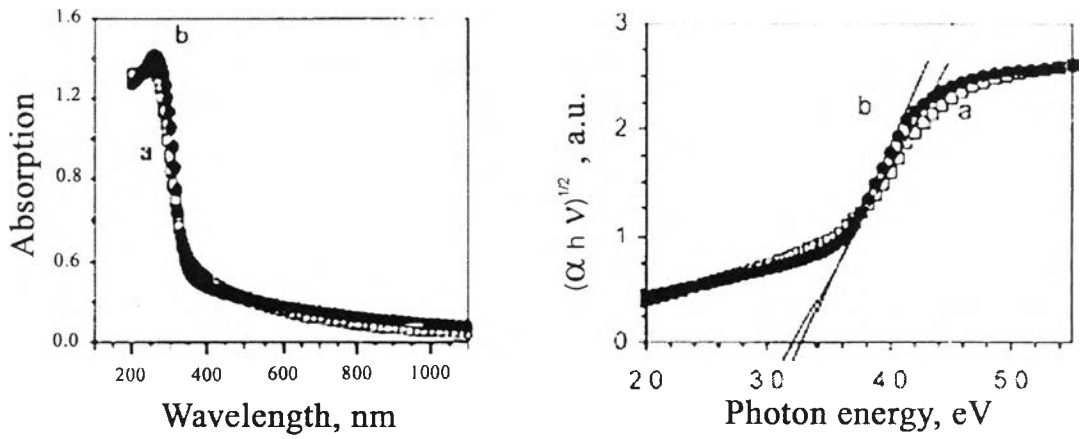

Fig. 2.9 Optical absorption spectra and $(\alpha\ h\ \nu)^{1/2}$ vs $h\ \nu$ curve, intercepts of (a) thin film $BaTiO_3$ and (b) annealed at 1000 °C.

Fig. 2.10(a) shows the variation in wavelength dependence of the photocurrent. The effect of heat treatment under nitrogen atmosphere and the doping effect of Ta[23] on the photocurrent were reported. The peak shifts and curves extension of the photocurrent in Fig. 2.10(b) were also noted in the wavelength dependence. The current peak for the nitrogen treated sample shifted to a shorter wavelength and simultaneously, the curve extended in the same direction, the peak of the photocurrent represented the band gap energy or absorption edge of these materials.

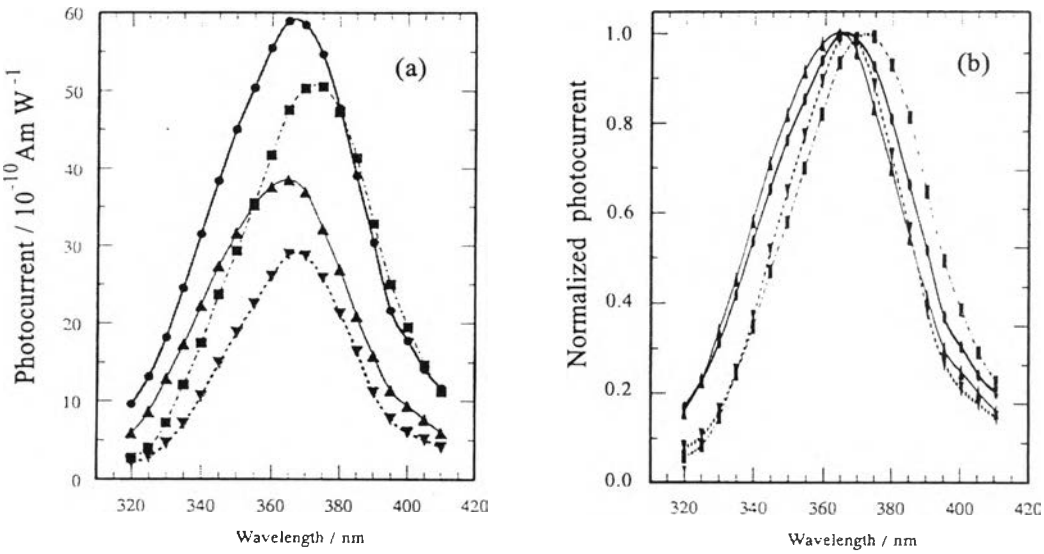

Fig. 2.10 Wavelength dependence of (a) photocurrent and (b) normalized photocurrent in the various samples : (▼) undoped PLZT (3/52/48), (▲) N_2 heat treated at 900 °C, (■) Ta doped, and (●) Ta doped and subsequently treated in N_2 at 900 °C.[23]

2.3 Piezoelectric effect

PLZT ceramics are currently focused because of their excellent piezoelectric properties, high piezoelectric constant (d_{33}) value.[1] Fig. 2.11 shows the contour map of the photovoltaic response and piezoelectric constant, d_{33}, on the PLZT phase diagram. The compositions around the morphotropic phase boundary (MPB) between the tetragonal and rhombohedral phases show the maximum d_{33} value. The maximum of d_{33} in Fig. 2.11 is about 700 x 10^{-12} m/V at the lanthanum content up to 8 mol%.

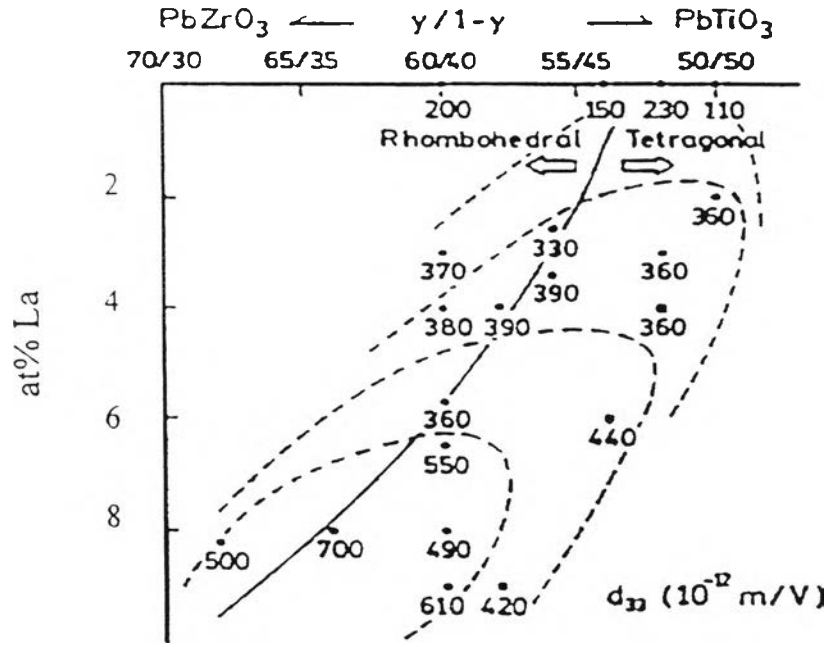

Fig. 2.11 Contour map of piezoelectric constant of PLZT ceramics

In PLZT (3/52/48) caramics system, small amount of dopant (1 at%) does not contribute to the piezoelectric effects in these materials. The value of piezoelectric constant remains constant. Fig. 2.12 shows that the piezoelectric constants of PLZT ceramics depend on the composition but not on the types of the dopants.[2]

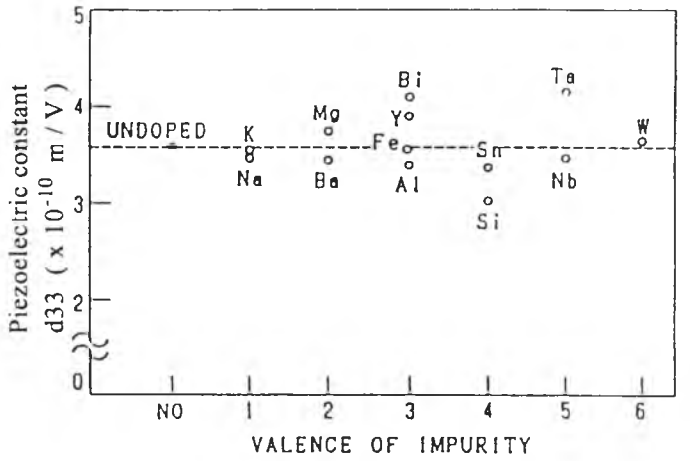

Fig. 2.12 Piezoelectric constants of PLZT ceramics (3/52/48) as a function of doping ions valency

2.4 Photostriction

Photostrictive effect is the combination of photovoltaic and piezoelectric effect. According to Eq. 1.1 :

$$x_{ph} = d_{33} \times E_{ph} \qquad (1.1)$$

where x_{ph} is photo-induced strain or photostriction
d_{33} is piezoelectric constant
and E_{ph} is photovoltage

In order to obtain a high photo-induced strain, materials with high d_{33} and E_{ph} are needed. Poosanaas[3] (1999) found the maximum strain in the composition of 5/54/46. Fig. 2.13 shows the contour map of photo-induced strain as a function of the composition of PLZT system. However, another factor required for the photostrictive effect is the response speed of the phenomenon. The response speed is defined as $(d_{33} \cdot I_{ph}) / C$ in the unit of sec^{-1}, when I_{ph} is photocurrent and C is the capacitance of the sample. The maximum response speed in PLZT system was found in the composition of 4/48/52. Fig. 2.14 shows the

contour map of response speed as a function of the composition of PLZT system. The photostrictive properties with the optimized requirement of figure of merit of photo-induced strain and response speed were found in the composition of 3/52/48 by Uchino in 1997[45], and Poosanaas in 1999.[3] It was obtained in the tetragonal region near the MPB with 3 mol% of Lanthanum which was also used in this study and doped with 0.5 at% of doping.

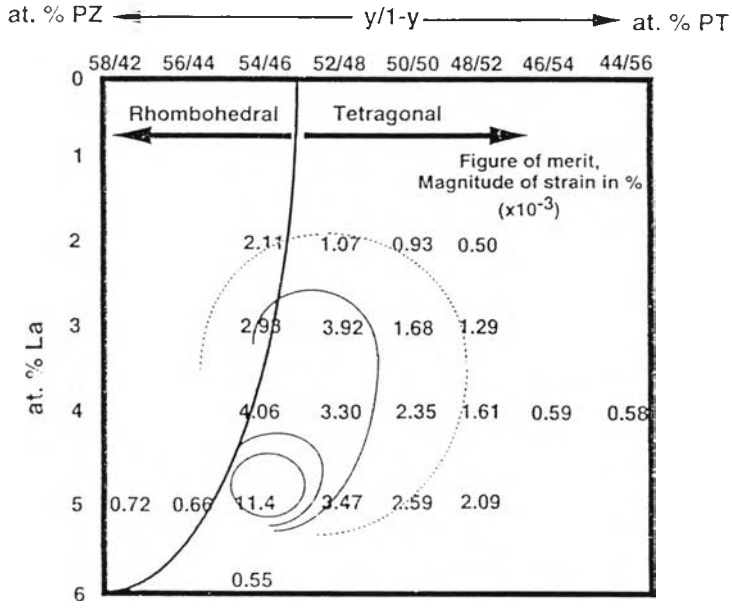

Fig. 2.13 The contour map of photo-induced strain of PLZT system

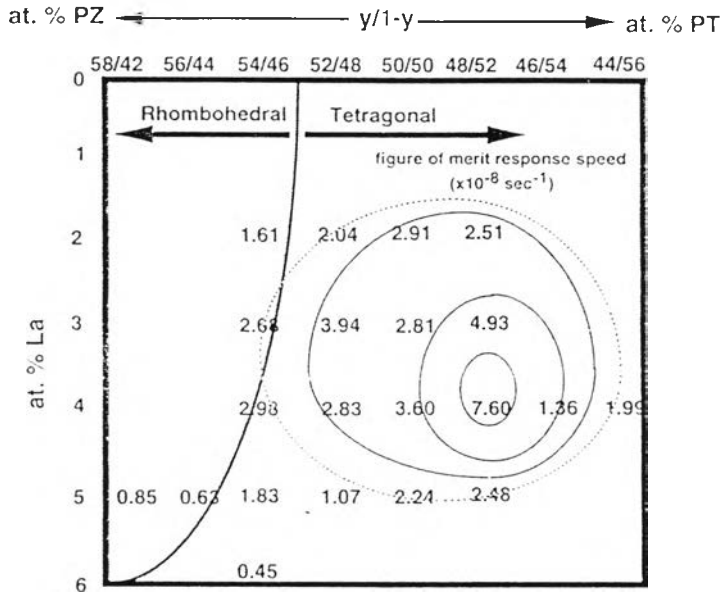

Fig. 2.14 The contour map of response speed of PLZT system